Pergamon

Geochimica et Cosmochimica Acta, Vol. 66, No. 2, pp. 347–359, 2002

0016-7037/02 $22.00 + .00

PII S0016-7037(01)00783-9

Iodine–Xenon dating of chondrules from the Qingzhen and Kota Kota enstatite chondrites

J. A. Whitby,[1,*] J. D. Gilmour,[1] G. Turner,[1] M. Prinz,[2] and R. D. Ash[2,†]

[1]Department of Earth Sciences, Manchester University, Manchester M13 9PL, United Kingdom
[2]Department of Earth and Planetary Sciences, American Museum of Natural History, Central Park West, New York, NY 10024, USA

(*Received July* 18, 2000; *accepted in revised form July* 20, 2001)

Abstract—Initial $^{129}I/^{127}I$ values (I-Xe ages) have been obtained for individual mineralogically characterized chondrules and interchondrule matrix from the enstatite chondrites Qingzhen (EH3) and Kota Kota (EH3). In view of the absence of aqueous alteration and the low-peak metamorphic temperatures experienced by these meteorites, we suggest that the I-Xe ages for the chondrules record the event in which they were formed. These ages are within the range recorded for chondrules from ordinary chondrites, demonstrating that chondrules formed during the same time interval in the source regions of both ordinary chondrites and enstatite chondrites. The timing of this chondrule-forming episode or episodes brackets the I-Xe closure age of planetesimal bodies such as the Shallowater aubrite parent body. Although chondrule formation need not have occurred close to planetesimals, the existence of planetesimals at the same time as chondrule formation provides constraints on models of this process. Whichever mechanisms are proposed to form and transport chondrules, they must be compatible with models of the protosolar nebula which predict the formation of differentiated bodies on the same timescale at the same heliocentric distance. *Copyright © 2001 Elsevier Science Ltd*

1. INTRODUCTION

Chondrules are spheroidal silicate objects widely distributed in the common chondritic meteorites (Hewins, 1994) and, by inference, were widespread in the early solar system. After rapid heating to near their melting point, they cooled at several hundred Kelvin per hour (Hewins et al., 1996); this requires a surrounding medium with an opacity greater than that of free space, perhaps due to a low-density cloud of hot dust and gas. No clear consensus for the environment in which they formed ("planetary" or "nebular") nor for a heating mechanism has yet emerged. Suggested mechanisms requiring a nebular environment have included lightning (Whipple, 1966; Horanyi et al., 1995), shock waves (Wood, 1984; Ruzmaikina and Ip, 1996; Connolly and Love, 1998), X-winds (Shu et al., 1996) and impacts between small objects (Kieffer, 1975); various authors have invoked parent-body scenarios for chondrule formation, usually involving impacts (Urey, 1967; Zook, 1980; Symes, 1997; Sanders, 1998), possibly induced by the gravitational influence of a newly formed Jupiter (Weidenschilling and Marzari, 1998). Theories of chondrule formation and alteration have been the subject of recent meetings, and the proceedings of these conferences form a useful review of the subject (Hewins et al., 1996; Zolensky et al., 1997).

A potentially important constraint on chondrule production scenarios is the timing of their formation. However, because the estimated lifetime of the solar nebula is 10 Ma or less (Podosek and Cassen, 1994; Hartmann, 1996; Wood, 1996, Briceno et al., 2001), to distinguish between nebular and early parent body scenarios requires high precision chronometric techniques; it is also vital to understand whether a given chronometer records primary crystallization of the minerals or a secondary alteration overprint. Few chronometers based on long-lived radionuclides have sufficient precision for such high temporal resolution measurements. However, short-lived radioisotopes allow high-precision relative dating of small samples such as chondrules and may enable us to disentangle the history of these objects and to distinguish between alternative scenarios for their formation. To be of use for this purpose, a chronometric system must have a temporal precision of at least 1 Ma (i.e., much less than the nebular lifetime), have a sensitivity appropriate for application to individual chondrules, and be readily interpretable. The radioactive decay of ^{129}I to ^{129}Xe ($\tau_{1/2}$ = 15.7 Ma) provides one such chronometer for the study of events in the early solar system (Reynolds, 1960). Iodine is widely distributed as a trace element in chondritic meteorites, the I-Xe system is readily examined in single chondrules, and a precision of better than 1 Ma can be achieved even on such small samples.

1.1. Iodine–Xenon Dating

Iodine–xenon dating employs the conversion of ^{127}I to ^{128}Xe by neutron capture during artificial irradiation, followed by isotopic analysis of the xenon released at various temperatures from the sample. Where a high-temperature correlation is observed between radiogenic $^{129}Xe^{*}$ and ^{127}I-derived $^{128}Xe^{*}$, the ratio of the two isotopes is used in conjunction with a standard to determine the $^{129}I/^{127}I$ ratio at the time the system closed to diffusive loss of xenon. The assumption of homogeneity in the primordial distribution of $^{129}I/^{127}I$ ratios at some stage then allows the calculation of relative radiometric ages for the closure event. Results from the I-Xe chronometer are usually quoted as relative ages with respect to either Bjurböle whole rock or, more recently, enstatite from Shallowater, which may conveniently be used as standards in the neutron irradiation

* Author to whom correspondence should be addressed, at Physikalisches Institut, University of Bern, CH3012 Bern, Switzerland (James.Whitby@phim.unibe.ch).
† *Present address:* Department of Earth Sciences, University of Oxford, Parks Road, Oxford OX1 3PR, UK.

step. Progress has however been made in correlating I-Xe ages with Pb-Pb ages, thus allowing absolute dating with the I-Xe system and establishing its consistency with other chronometers (Nichols et al., 1994; Brazzle et al., 1999; Gilmour, 2000; Gilmour and Saxton, 2001).

Previous work has shown a considerable spread in I-Xe ages for chondrules from carbonaceous and low-petrologic-type ordinary chondrites (Nichols et al., 1990; Swindle et al., 1991a,b). Rather than interpret these as chondrule formation ages, the authors suggested that they dated either aqueous alteration (e.g., Semarkona LL3.0) or disturbances due to shock (e.g., Chainpur LL3.4). In an attempt to avoid similar difficulties in interpretation, we have selected samples from the unequilibrated EH chondrites Qingzhen (EH3) and Kota Kota (EH3), which are believed to have had simpler geological histories than their counterparts in other groups.

1.2. Enstatite Chondrites

The enstatite chondrites in general show very little evidence of preterrestrial aqueous alteration and petrologic types 3 and 4 do not seem to have been subject to metamorphic temperatures much in excess of 700°C (Dodd, 1981; Zhang and Sears, 1996), although textural and mineralogical features appear to record different aspects of the thermal history of enstatite chondrites (Zhang et al., 1995). The EH3 chondrites in particular have not been heated above 507°C (on the basis of the presence of copper sulfide; El Goresy et al., 1986), and metamorphism is more likely to have occurred in the range 300 to 400°C (El Goresy et al., 1986). They are thus expected to have retained chronometric information about the initial formation of high-temperature phases within them. Qingzhen and Kota Kota have both been classified as shock stage 3—that is, weakly shocked to ~10 GPa (Rubin et al., 1997). Possible effects of aqueous alteration, metamorphism and shock on the iodine–xenon system are discussed below in section 4.1.

Previous work has demonstrated that both ^{129}I with a half-life of 15.7 Ma (Kennedy et al., 1988) and ^{53}Mn with a half-life of 3.7 Ma (Wadwha et al., 1997) were still present when host phases became closed to isotopic exchange of these systems in low-petrologic-type EH chondrites. The host phase for radiogenic xenon (from ^{129}I) is not known for certain, but ^{129}Xe* in EL6 chondrites is associated mainly with enstatite, and in EH3 and EH4 chondrites, it is associated with chondrules, phases soluble in HCl, and a fine-grained, HCl-insoluble, low-density component (Crabb and Anders, 1981, 1982). Evidence for ^{53}Mn has been found in sphalerites in Indarch (EH4) but no excess of ^{53}Cr (from ^{53}Mn) has been found in sphalerite or niningerite from Qingzhen or in sphalerite from Kota Kota (Wadwha et al., 1997).

Qingzhen and Kota Kota were selected for this study because other EH3 chondrites exhibit various degrees of weathering and terrestrial alteration that it was felt might have introduced iodine in sufficient abundance to complicate I-Xe studies. In particular, most of the ~50 known EH3 meteorites have been recovered from the Antarctic, an environment demonstrated to introduce iodine (Langenauer and Krähenbühl, 1993). Qingzhen is an observed fall from 1976 (Wang and Xie, 1982), and Kota Kota was reported to have fallen some years before 1905 (Prior, 1914). Although Kota Kota has been reported as badly weathered (Mason, 1965), with alteration products present in the fine-grained rims around chondrules (Leitch and Smith, 1982), there is no mineralogical evidence of alteration in the chondrules selected for this study. Neither our samples of Qingzhen nor of Kota Kota show any preterrestrial aqueous alteration, and both still contain readily water-soluble sulfides such as oldhamite, suggesting that terrestrial weathering has had little effect. The presence of hydrated iron–chromium sulfides in the matrix of Qingzhen has been reported (El Goresy et al., 1986, 1988), but these were not observed in any of the chondrule samples used in this work.

2. ANALYTICAL PROCEDURES

2.1. Sample Preparation

Eight chondrules (QC1 to QC8) and five pieces of matrix (QM1 to QM5) from Qingzhen and four chondrules (KC1 to KC4) and five pieces of matrix (KM1 to KM5) from Kota Kota were extracted from hand specimens with dental tools. Chondrules were recognized by their structure; matrix samples represent the poorly characterized, generally fine grained material found between chondrules and metal-sulfide assemblages, which may in part consist of comminuted chondrules. Superfluous adhering material was removed from the chondrules, which were then rinsed with acetone before being weighed and cleaved into two or more pieces. The largest piece of each chondrule was included in neutron irradiation MN9 in the rodeo position of the Petten reactor (fast fluence of 6.0×10^{18} neutrons cm^{-2}, thermal fluence 3.5×10^{19} neutrons cm^{-2}), whereas the remainder was retained for mineralogical and petrological characterization with electron microprobe stub mounts. The matrix samples were not split and were irradiated in their entirety.

Petrographic analyses were carried out with a JEOL JSM-840A scanning electron microscope by means of both photomicrography and low-resolution element mapping. Element maps were digitally combined to produce images from which mineral abundances could be derived. Mineral chemical analyses were obtained with the Smithsonian Institution's JEOL JXA-8900R electron microprobe, and cathodoluminescence studies were made with an ELM-3R luminoscope.

Unfortunately, chondrule sample KC3 was lost as the irradiated samples were prepared for loading into the mass spectrometer, and only the matrix sample KM2 was analyzed because the other Kota Kota matrix samples had become extremely fragile during the irradiation and were difficult to handle safely.

2.2. Xenon Analysis

Xenon isotope analysis was carried out with the RELAX laser resonance ionization time-of-flight mass spectrometer (Gilmour et al., 1994) in conjunction with laser-stepped heating of the samples. To heat the samples, the beam from a Nd:YAG continuous wave laser ($\lambda = 1064$ nm) with a gaussian (TEM_{00}) spot of approximately 3-mm diameter was used (considerably larger than the samples); heating was for 60 s at each step with laser beam powers from 0.1 to 9 W. Accurate sample temperatures are hard to measure or calculate, but an estimate can be made by equating the incoming laser power to heat loss by

thermal radiation by use of Stefan's Law. Previous work based on comparison with filament-stepped heating experiments has shown this to yield reasonable estimates at high temperature (Gilmour et al., 1998). This procedure suggests that the high end of the power range corresponds to more than 1700°C. All samples were heated to beyond the point at which they melted, thus ensuring that all gas was released. Temperature gradients across the sample are believed to have been small compared with the temperature steps, resulting in well-resolved stepped-release profiles.

A data collection cycle consisted of an atmosphere-derived calibration aliquot (8×10^{-15} cm^3 ^{132}X at Standard Temperature and Pressure), then a blank measurement, three stepped-heating measurements, and another calibration aliquot. Each measurement involves collecting data for 3000 ionization cycles (5 min) as sets of time-of-flight spectra averaged 100 cycles (10 s) each. Blanks were less than 1×10^{-16} cm^3 STP ^{132}Xe throughout the period in which this work was carried out. The atmospheric aliquots bracketing the sample analyses were used to correct for instrumental mass discrimination and to account for minor fluctuations in sensitivity.

Aliquots of both a nonmagnetic fraction from the aubrite Shallowater and whole-rock portions of Bjurböle were included in the irradiation as iodine standards (Brazzle et al., 1995; Gilmour et al., 1997), and the hornblende standard Hb3gr (Turner, 1971; Roddick, 1983) was also used as a fluence monitor. No measurable difference in fluence was observed among the Shallowater standards or hornblende monitors. The conversion factor for ^{127}I(n,β^-)^{128}Xe was calculated directly from the known initial iodine ratio of the Shallowater standard (Hohenberg, 1967); factors for ^{130}Ba(n,e-capture)^{131}Xe, ^{130}Te(n,2β)^{131}Xe and the xenon yield from neutron-induced fission of uranium were calculated by means of the measured fluences and published neutron capture cross sections, branching ratios, and fission yields (General Electric, 1988; Ozima and Podosek, 1983).

2.3. Data Reduction

After neutron irradiation, xenon in chondritic meteorites is a mixture of isotopically distinct components. To decompose this mixture, ^{132}Xe was apportioned between "planetary" and fission components by use of the measured ^{134}Xe/^{132}Xe ratio and the values of Wieler et al. (1992) for a trapped planetary component and those of Ozima and Podosek (1983) for the induced fission component. (The fission correction was small and the choice of induced uranium fission xenon or spontaneous plutonium fission xenon as the end member made no difference to the ^{129}Xe/^{128}Xe correlations.) The fission-corrected ^{132}Xe value representing the amount of planetary xenon is denoted ^{132}Xe$_P$. Excesses of ^{128}Xe and ^{131}Xe produced by neutron irradiation were calculated over the trapped component (assumed to be of planetary composition except where otherwise noted); the excess of ^{131}Xe was then corrected for an induced fission contribution to give the amount of ^{131}Xe due to neutron capture by ^{130}Ba and ^{130}Te. These irradiation produced excesses are denoted by ^{128}Xe* and ^{131}Xe*. A similar procedure was followed to obtain the excess of ^{129}Xe denoted by ^{129}Xe*. Three-isotope plots among ^{129}Xe, ^{128}Xe* and ^{132}Xe$_P$ were then used to seek a correlation between iodine-derived ^{128}Xe* and excesses of ^{129}Xe. Where these were present, line fits (which used an appropriate least-squares fitting procedure; York, 1969) were employed to derive the initial ^{129}I/^{127}I ratio and the ^{129}Xe/^{132}Xe ratio of any accompanying trapped (i.e., nonradiogenic) component.

^{129}I/^{127}I ratios have been determined by using the Shallowater enstatite achondrite as a standard (^{129}I/^{127}I = $1.125 \pm 0.012 \times 10^{-4}$; Hohenberg, 1967), it having been demonstrated that Shallowater is a more reproducible standard (McCoy et al., 1995; Gilmour et al., 1997) than Bjurböle (^{129}I/^{127}I = 1.095×10^{-4}; Hohenberg and Kennedy, 1981) when small quantities (~1 mg) are used. Enstatite from Shallowater has a reproducible ^{129}I/^{127}I value, whereas chondrules from Bjurböle exhibit a range of values (Caffee et al., 1982b; Gilmour et al., 1997). Samples of Shallowater and Bjurböle whole rock that have been irradiated together are reported as having varying fractional differences in their initial iodine ratios (Kehm et al., 1993; Brazzle et al., 1995; McCoy et al., 1995), all of which are different from the value obtained by considering the absolute values given earlier. It seems reasonable to ascribe this variation to the observed distribution of initial iodine values of chondrules within Bjurböle.

For consistency with previously published work concerned with I-Xe dating, a half-life for ^{129}I of 15.7 Ma has been adopted when discussing age differences (Emery et al., 1972), although 17 Ma has been suggested as a more appropriate value (Holden, 1990). By use of the literature values given above, bulk Bjurböle is calculated to have an I-Xe closure age some 0.6 Ma later than bulk Shallowater, although the difference is not statistically significant in this case. It should be borne in mind that a systematic error in the initial iodine isotope ratio assigned to Shallowater (due to the difficulties of measuring absolute production rates of ^{128}Xe from ^{127}I), as has been suggested possible by Hohenberg et al. (2000), will result in all ^{129}Xe/^{127}I and inferred ^{129}I/^{127}I values reported in this work being similarly in error. Nevertheless, provided ratios (and ages) are referred to a common monitor, preferably Shallowater or Bjurböle, then the effect of any systematic error would be to scale reported Xe/I ratios uniformly, resulting in a constant offset for inferred ages. We believe it is essential to use correlation plots based on ^{129}Xe, ^{132}Xe and the inferred ^{127}I, rather than on ^{129}Xe, ^{132}Xe and ^{128}Xe. Unless this is done it is difficult to compare data from different laboratories and irradiations. The idea that it is sufficient to compare inferred relative ages is flawed in that it ignores the additional information present in isotope correlation diagrams.

3. RESULTS

Petrographic descriptions of the chondrule fragments are summarized in the Appendix, and their significance for the interpretation of the I-Xe system is discussed in section 4.1. Although the proportion of textural types sampled is not a good match with the distribution observed in the bulk of Qingzhen (Johnston, 1995), each of the major types is, however, represented.

Sample masses and data from xenon analyses are presented in Table 1. Where barium and tellurium are present in chondritic abundances (Anders and Grevesse, 1989), tellurium dominates ^{131}Xe* production. However, our chondrule samples do

Table 1. Summary of initial iodine ratios, 1-Xe ages, and iodine, tellurium/barium, and uranium abundances for all samples.[a]

Sample	Chondrule mass (μg)	Analyzed mass (μg)	^{129}Xe cm^3 STP/g ($\times 10^{12}$)	$^{132}Xe_p$ cm^3 STP/g ($\times 10^{12}$)[b]	[I]ppb	[Te]ppb[c]	[Ba]ppb[c]	[U]ppb	^{129}I/^{127}I ($\times 10^4$)[d]	^{128}Xe (%) [e]	Age/Ma[f]
QC1	2180	1410	170	8.3	10	15	140	1.4	1.13 ± 0.023[g]	—	−0.1 ± 0.56[g]
QC2	570	300	110	23	6.5	1700	15000	6.0	1.15 ± 0.029	77	−0.45 ± 0.57
QC3	1280	570	360	22	19	81	730	7.2	1.11 ± 0.013	56	0.33 ± 0.26
QC4	740	330	240	18	11	110	980	10	1.17 ± 0.013	88	−0.95 ± 0.25
QC5	170	170	310	12	18	61	550	4.5	1.06 ± 0.029	86	1.26 ± 0.62
QC6	3790	790	190	30	10	14	130	5.3	1.12 ± 0.013	85	0.19 ± 0.26
QC7	720	160	850	35	46	790	7100	21	1.07 ± 0.019[h]	74	1.20 ± 0.41[h]
QC8	7720	3830	190	5.9	11	52	470	1.5	1.04 ± 0.013	87	1.68 ± 0.28
QM1	—	320	39	28	2.8	22	200	2.1	—	—	—
QM2	—	710	140	4.3	8.3	59	540	2.9	—	—	—
QM3	—	190	170	120	22	160	1400	8.8	—	—	—
QM4	—	1170	160	140	10	60	540	3.5	—	—	—
QM5	—	500	140	210	12	63	570	10	—	—	—
KC1	2070	880	170	15	12	29	260	3.7	1.10 ± 0.026	37	0.46 ± 0.53
KC2	1550	180	320	70	18	160	1500	13	1.13 ± 0.029	80	−0.13 ± 0.58
KC4	1720	470	44(11)[i]	230	1.9	360	3300	6.5	—	—	—
KM2	—	550	90	120	6.0	26	240	3.6	—	—	—

[a] The data in Table 1 are slightly different from those reported by us in earlier abstracts of this work (Ash et al., 1997; Whitby et al., 1997) as a result of a more complete analysis of the results. In particular, QC1 does not exhibit a satisfactory isochron, QC2 had not been fully analyzed and the highest temperature datum for QC7 has now been omitted from the fit (see Fig. 2a). [b] Planetary component; see text. [c] Coupled upper limits; see text. [d] Calculated by using Shallowater $^{129}I/^{127}I = 1.125 \times 10^{-4}$. [e] Fraction of iodine-derived xenon in correlation line. [f] I-Xe age relative to Shallowater using half-life of 15.7Ma. [g] Based on single large highest temperature release. [h] Highest-temperature datum omitted. [i] Figure in brackets calculated using trapped component with $^{129}Xe/^{132}Xe = 1.18$.

not necessarily have chondritic abundances. No significant spallation component was detected, so correlation with spallation-produced ^{124}Xe and ^{126}Xe could not be used to attribute $^{131}Xe^*$ to barium; it was thus impossible to distinguish between barium or tellurium as the parent of $^{131}Xe^*$, so derived concentrations of these two elements in Table 1 are upper limits, each calculated on the assumption that only one of them was present.

3.1. Qingzhen

In all Qingzhen samples, the trapped xenon component inferred from three-isotope plots had a $^{129}Xe/^{132}Xe$ ratio consistent with that of the ordinary chondrite ($^{129}Xe/^{132}Xe = 1.040$; Lavielle and Marti, 1992) or Q-trapped components ($^{129}Xe/^{132}Xe = 1.036$; Wieler et al., 1992), so the former composition was used to calculate excess ^{129}Xe ($^{129}Xe^*$) from decay of ^{129}I. The matrix samples generally had higher abundances of trapped planetary xenon than the chondrules, as previously observed by Whitby et al. (1998) for a Saharan EH3 and as suggested by the data of Crabb and Anders (1982) for size/density separated fractions of Qingzhen. (The matrix is finer grained than that of the chondrules.) Iodine, uranium, and tellurium or barium (Table 1) are more abundant in chondrules from Qingzhen than in the matrix, but correlation between these elements is poor, suggesting that more than one host phase is responsible.

The uranium concentrations for Qingzhen chondrules of 1 to 21 ppb found in this work bracket the whole-rock value of 8.2 ppb (Kaczaral et al., 1988). These values are consistent with the observed 1 to 6% abundances of sulfide minerals (Appendix) if it is assumed that the uranium concentration in troilite and other sulfide minerals present is not very different from the mean concentration of uranium in oldhamite from Qingzhen of 300 ppb (Rambaldi et al., 1984), and that uranium is predominantly hosted by sulfide minerals. Crystallites in glassy mesostasis in some chondrules from Qingzhen have also been shown to have locally high (140 ppb) uranium concentrations (Rambaldi et al., 1984) and would lead to uranium concentrations in chondrules higher than expected from contributions from oldhamite alone.

Stepped heating of the chondrules shows that the endogenous and trapped gases have different release patterns, suggesting that they are hosted by different minerals. Trapped xenon is released from synthetic enstatite at lower temperatures than iodine-derived xenon (Zaikowski et al., 1979), but this does not explain all the patterns observed. Furthermore, although the release patterns for each of the endogenous components are similar within a given chondrule, in detail, the proportions within and between chondrules differ. These results suggest that although the endogenous components (e.g., xenon derived from iodine, barium, tellurium, and fission) may not be hosted by the same mineral, they are nevertheless subject to the same controls on diffusion path lengths, perhaps due to minor phases included within a host with a higher melting point (e.g., enstatite). Alternatively, there may be a host mineral common to each chondrule, but with varying trace-element chemistry. In contrast, the release patterns from the matrix samples show all xenon components behaving similarly, perhaps as a result of the finer grain size. Previous work (Crabb and Anders, 1982) suggests that enstatite hosts a significant fraction of the radiogenic ^{129}Xe in bulk Qingzhen and is likely to be responsible for the high temperature release; this is consistent with observations that $^{129}Xe^*$ is associated with enstatite in the Yilmia EL6 chondrite (Crabb and Anders, 1982), the Indarch EH4 chondrite (Wacker and Marti, 1983), and the Shallowater aubrite (Kehm et al., 1994).

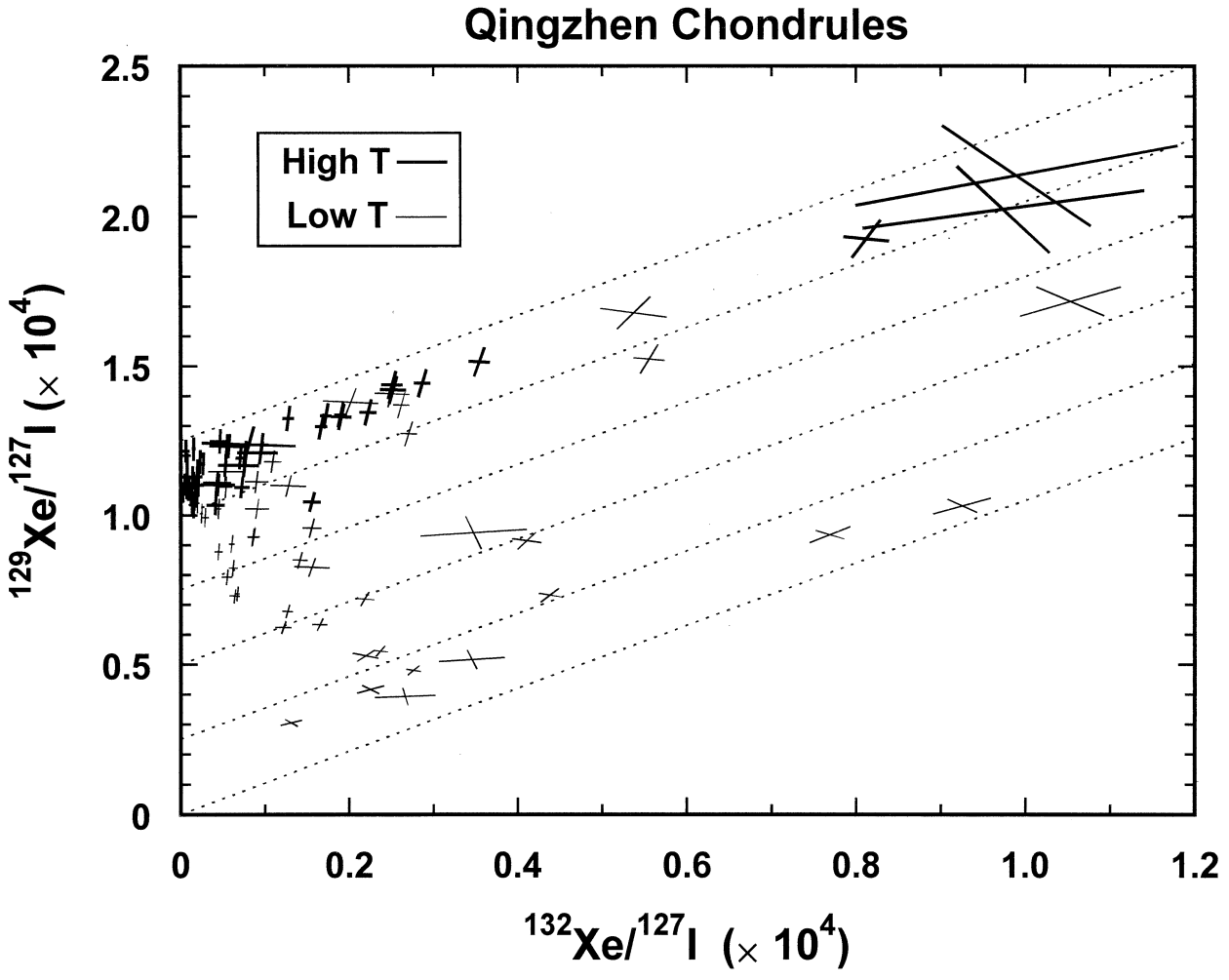

Fig. 1. Three-isotope plot for all Qingzhen chondrule samples. A purely iodine-derived xenon component plots on the y-axis; mixing with a planetary xenon component moves points diagonally up and to the right, parallel to the dotted lines (which assume $^{129}Xe/^{132}Xe = 1$). High temperature points define a line with $^{129}Xe/^{132}Xe \sim 1$ consistent with a trapped planetary component in each chondrule; the fairly well defined intercept and mixing line graphically demonstrate the narrow range of ages in the chondrules. The low temperature points fall below this mixing line as a result of the addition of iodine with a lower initial $^{129}I/^{127}I$ ratio. Terrestrial iodine mixing with terrestrial air would result in an array of points lying on a line passing through the origin with slope similar to that indicated by the dotted line.

Seven of the eight Qingzhen chondrules analyzed gave well defined high-temperature initial iodine ratios (Table 1 and Figs. 1 and 2). Figure 2 shows initial iodine ratios plotted against fractional iodine release (analogous to Ar-Ar age spectra) because the relatively small amounts of trapped planetary xenon released at high temperatures render conventional three-isotope isochron plots uninformative. Chondrule QC1 did not exhibit a good correlation between ^{128}Xe and ^{129}Xe, but the high temperature release accounting for 50% of the iodine-derived $^{129}Xe^*$ had a value of $^{129}I/^{127}I = 1.13 \times 10^{-4}$, similar to the other chondrules. If these initial iodine ratios are interpreted as formation ages, then they correspond to a range of 2.6 Ma, with a mean value indistinguishable from closure in the Shallowater enstatite achondrite. The matrix samples from Qingzhen did not give such well defined initial iodine values, and two were clearly disturbed, however the other three samples of matrix gave initial iodine values similar to those observed in the chondrules. It may be that where an aliquot of matrix material gives a well-defined initial iodine value, this is due to a fragment of a chondrule or some other discrete object dominating the xenon composition.

Some of the Qingzhen chondrules appeared to contain a xenon component released at low temperatures (600 to 800°C) that had a measurable $^{129}Xe/^{127}I$ excess ratio much lower than that derived from the remaining temperature steps. This component can be seen in Figure 1, which shows data for all the Qingzhen chondrules on a three-isotope plot. It can also be seen as an indistinct shoulder on plots of $^{129}Xe^*/^{128}Xe^*$ vs. cumulative $^{128}Xe^*$ in Figures 2a and 2b. It is quite common in stepped-heating I-Xe studies for low-temperature releases to consist mostly of ^{128}Xe derived from ^{127}I during the neutron irradiation; this is usually interpreted as arising either from terrestrial iodine contamination or from late closure (i.e., after decay of all ^{129}I) of low-temperature iodine-bearing phases.

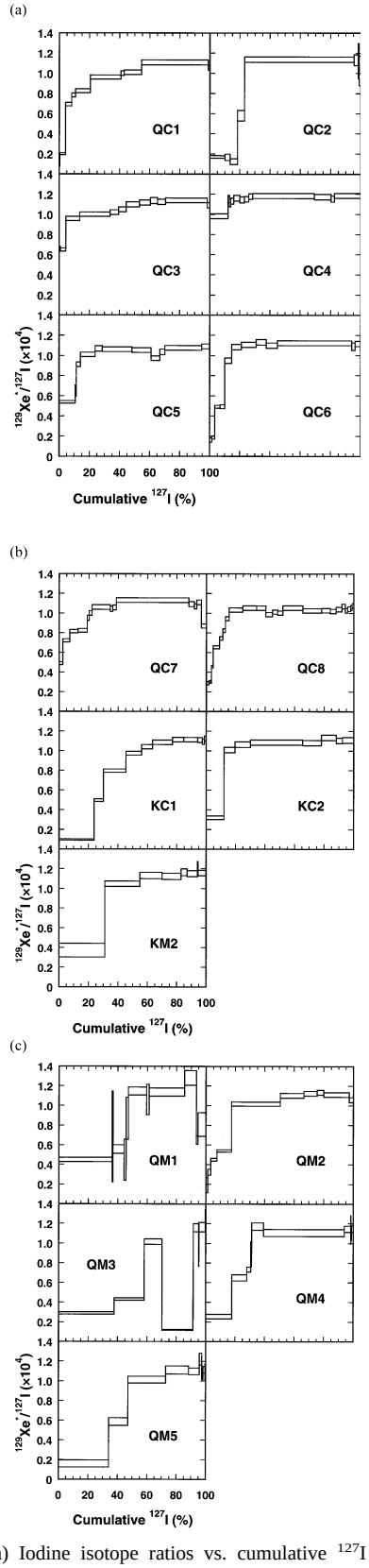

Fig. 2. (a) Iodine isotope ratios vs. cumulative ^{127}I released by stepped heating for chondrules QC1-QC6. (b) Iodine isotope ratios vs. cumulative ^{127}I released by stepped heating for QC7, QC8, KC1, KC2, and KM2. (c) Iodine isotope ratios vs. cumulative ^{127}I by stepped heating for all Qingzhen matrix samples QM1 to QM5.

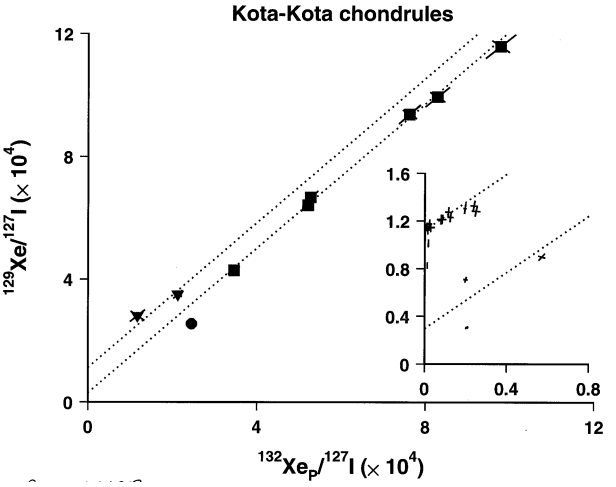

Fig. 3. Three-isotope plot for chondrule KC4 demonstrating trapped xenon component with elevated $^{129}Xe/^{132}Xe$. Solid triangles denote the two highest-temperature gas releases; solid squares denote the midtemperature releases. Inset is an expanded view showing data from chondrules KC1 and KC2. See text for discussion.

Because Qingzhen chondrules clearly released excess ^{129}Xe in the low-temperature component, it is not due solely to terrestrial iodine contamination and raises the possibility of some alteration event or disturbance having been recorded in these samples while some ^{129}I still existed.

An alternative explanation is that there has been an incomplete separation of a nonradiogenic low-temperature component and a higher temperature radiogenic ^{129}Xe-bearing component. Stepped-heating release patterns for the Shallowater aubrite (used as a standard in this work) where the host phase for iodine is believed to be enstatite (Kehm et al., 1994) show a clearer separation between a low-temperature, pure ^{127}I-derived component and a high-temperature component with a single $^{129}Xe^{*}/^{128}Xe^{*}$ value. That the two components are not clearly separated in the Qingzhen chondrules supports the presence of one or more mineral phases, with low-closure temperatures hosting ^{129}I-derived xenon that are not resolved from a pure ^{127}I-derived low-temperature component.

3.2. Kota Kota

Two of the three chondrules from Kota Kota (KC1 and KC2) gave good initial iodine values indistinguishable from that of the Shallowater standard; the matrix sample (KM2) was also within error of the standard (Table 1 and Fig. 2b). A previous whole-rock study (Kennedy et al., 1988) did not yield a satisfactory isochron, so these are the first model-independent iodine–xenon ages obtained for Kota Kota. In each case, the $^{129}Xe/^{132}Xe$ ratio of the trapped xenon was again indistinguishable from the ordinary chondrite planetary or Q component.

The situation for the third chondrule KC4 is more complicated. Figure 3 is a three-isotope plot of total ^{129}Xe, ^{127}I (inferred from $^{128}Xe^{*}$), and the planetary component of ^{132}Xe. In this plot, if data fall on a line, then the y-intercept corresponds to the initial iodine ratio (or age), and the gradient gives the $^{129}Xe/^{132}Xe$ value for the trapped component. A generally poor correlation between total ^{129}Xe and $^{132}Xe_P$ is observed,

yet six midtemperature releases give a well-defined array of points with a gradient corresponding to a trapped xenon component with $^{129}Xe/^{132}Xe = 1.18 \pm 0.03$, significantly higher than the ordinary chondrite value of $^{129}Xe/^{132}Xe = 1.04$. A line through these midtemperature points intercepts the y-axis to give an initial iodine value of $^{129}I/^{127}I = 3 \times 10^{-5}$, corresponding to a closure age 30 Ma later than Shallowater. If a line with the former gradient is fitted to the last two (high temperature) releases, it intercepts the y-axis at a value corresponding to an initial iodine value similar to those of KC1 and KC2 (i.e., the same I-Xe closure age as Shallowater).

Chondrule KC4 is rich in trapped xenon, with a concentration of trapped ^{132}Xe an order of magnitude greater than any of the other chondrules studied in this work, and actually greater than any of the matrix samples from either Qingzhen or Kota Kota. The iodine concentration is the lowest of any of the chondrule or matrix samples reported here, and the resulting $^{127}I/^{132}Xe$ ratio of $\sim 1 \times 10^3$ is much less than the values for enstatite chondrite chondrules or whole-rock of $\sim 1 \times 10^5$. Because there is nothing unusual about the grain size or petrology of this chondrule, it seems likely that the trapping of the evolved component took place in the presence of a partial pressure of xenon considerably in excess of that experienced by other samples in this suite.

Our favored interpretation of these observations is that chondrule KC4 experienced an event that injected a xenon component with an evolved $^{129}Xe/^{132}Xe$ ratio and probably resulted in the loss of some iodine. As a result of this disturbance, the I-Xe system in most phases within the chondrule was reset, dating the event at $\sim$30 Ma later than closure in Shallowater. The two highest-temperature gas releases seem to record an earlier age, suggesting that they were not completely reset by this event. If the phase responsible for the earlier ages was not reset, it should not have acquired the same evolved trapped component. There may, however, have been a degree of mixing between the different components due to diffusion during the high-temperature releases, which are therefore only indicative of a formation age similar to chondrules KC1 and KC2. Although the chondrule has clearly been disturbed subsequent to its initial formation, there is no petrological evidence for aqueous alteration or very high shock pressures (Appendix). However, with only a probe mount of the sample, it is impossible to assess shock effects below about shock stage S5 because the criteria require the use of transmitted light (Stöffler et al., 1991; Rubin et al., 1997).

4. DISCUSSION

4.1. Setting of EH3 Chondrule Initial Iodine Ratios

The chondrules studied in this work show no uniform petrological evidence for aqueous alteration or significant metamorphism (Appendix). There is evidence that both carbonaceous and ordinary chondrites have undergone aqueous alteration, but the enstatite chondrites have done so to a much lesser or negligible extent. For example, the presence of clay minerals and biopyriboles in the least metamorphosed members of the carbonaceous and ordinary chondrite groups are common features observed by transmission electron microscopy, but in general, the enstatite chondrites do not contain hydrated minerals, thus indicating a paucity of water. (The matrix of Qingzhen has however been reported to contain iron-chromium sulfides with low analytical totals that are inferred to be due to hydration; El Goresy et al. 1986, 1988.) The briny fluids of the carbonaceous and ordinary chondrites also facilitated iron metasomatism, as shown by the presence of nonigneous iron zoning within silicates in these rocks, and iron enrichments at the edges of chondrules and isolated silicate grains. Conversely, iron in the enstatite chondrites is largely present as a sulfide or metallic phase and, where it is present in silicates, exhibits little zoning. Leaching of feldspathic chondrule glass in carbonaceous and ordinary chondrites is also attributable to dissolution by flowing water, a feature not observed in enstatite chondrite chondrules. Enstatite chondrites also lack carbonate or sulfate veins, a common feature in carbonaceous and, more rarely, ordinary chondrites. These are the result of saturated fluid flow through the chondrite parent bodies.

The enstatite chondrites are the most reduced of the chondrite groups, with normally lithophile elements forming sulfide minerals (e.g., oldhamite, alabandite, niningerite) rather than silicates. These sulfides are generally highly soluble in water and readily react with carbon dioxide to produce carbonates. The ease of decomposition of these minerals during terrestrial weathering is well documented (El Goresy et al., 1988; Rubin, 1997) and the presence of these sulfides, as primary minerals within the enstatite chondrites, attests to the lack of significant water or carbon dioxide fluid flow within the enstatite chondrite parent body.

The enstatite chondrites in general, and the chondrules examined in this study in particular, show none of the features mentioned above that would suggest hydrothermal alteration was ever an important feature of the history of these rocks. They contain primary readily soluble sulfides such as oldhamite and so cannot have been exposed to an abundant aqueous fluid.

Sodium, chlorine, and potassium show highly variable enrichments in some chondrules (particularly QC1 and QC2). These enrichments are associated with cracks and grain boundaries in the mesostasis, suggesting a postcrystallization diffusion controlled influx of these elements. This may be interpreted as having occurred immediately after the high-temperature formation of the chondrules (and thus having had no effect on the ages defined by the I-Xe chronometer), or at a later date, perhaps from a fluid on a parent body. Neither of these chondrules shows any increase in iodine concentration compared to the other Qingzhen chondrules in this study, nor do they appear unusual in their xenon concentration, the shape and quality of their age spectra, or their inferred initial iodine isotope ratios. It would appear therefore that any postformation influx of light alkali and halogen elements has had no observable effect on the I-Xe system.

The low metamorphic temperatures experienced by the unequilibrated EH chondrites would not have allowed significant xenon exchange, and so postaccretion thermal episodes do not account for the I-Xe ages of the chondrules. All the chondrules in this study still contain glass except QC6, suggesting the absence of any prolonged heating after formation.

Although the K-Ar and Rb-Sr systems show evidence of a late alteration episode in Qingzhen at 2 Ga (Jessberger, 1983; Müller and Jessberger, 1985; Torigoye and Shima, 1993), which has affected some minerals in the matrix, especially djerfisherite (El Goresy et al., 1988), other phases have been

less affected, particularly those within chondrules. The high proportion of iodine-derived ^{128}Xe that correlates with ^{129}Xe* (Table 1) is also a clear indication that there has been little interaction of the chondrules with fluids since the event dated by the I-Xe closure age.

Shock effects are unlikely to account for the observed I-Xe ages because both Qingzhen and Kota Kota are classified as shock stage S3 (Rubin et al., 1997), which would not have led to much loss of trapped xenon, nor to a significant rise in temperature (Stöffler et al., 1991). Furthermore, shock-induced redistribution of iodine or xenon tends to reduce the range of iodine/xenon ratios (Caffee et al., 1982a), which is not consistent with the very high peak iodine/xenon ratios observed in the high temperature releases responsible for the I-Xe correlation in these samples. Additionally, the distinct release patterns for trapped planetary xenon and the radiogenic component, coupled with the high precision of the isochrons, make shock disturbance an implausible explanation of the observed I-Xe ages for the majority of the chondrules in this study.

It was suggested to us that the rims of the chondrules could have a different initial iodine ratio than the cores and that the rims might be the source of the iodine-derived xenon observed at high-temperature steps, as suggested by Nichols et al. (1990). However, the uniformity of initial iodine ratios observed over multiple temperature steps for any one chondrule and the typically large fraction of ^{127}I-derived xenon included in the correlation (Table 1) argue against multiple iodine ratios within a chondrule. Furthermore, fine-grained external material would be expected to degas at lower temperatures than the core of a chondrule.

In summary, there is, with the possible exception of KC4, no evidence for any event that would have opened the phases responsible for high temperature xenon releases during stepped heating to xenon re-equilibration since their formation. We therefore conclude that initial iodine isotope values of chondrules from these unequilibrated EH chondrites were last reset by the high-temperature formation of the chondrules.

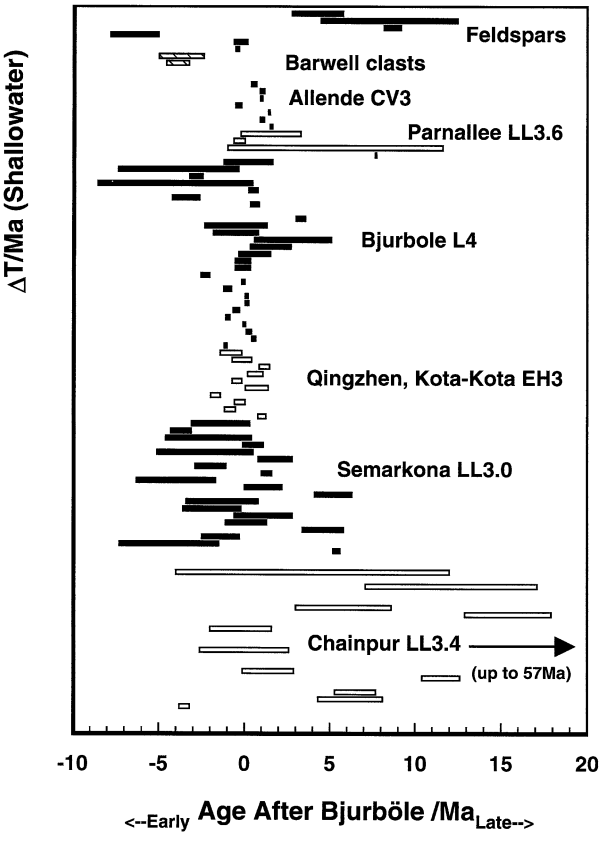

4.2. Interpretation of Initial Iodine in Chondrules

Broadly similar initial iodine isotope values have been obtained for chondrule formation by using chondrules from different groups of meteorites (Fig. 4). Because these groups represent chemically distinct parent bodies thought to have formed at different radii from the sun, any spatial inhomogeneity in ^{129}I/^{127}I ratios can only have been minor and of no significance to I-Xe studies at their current level of precision. Previous studies of the iodine–xenon system within individual chondrules have resulted in a range in ages, often interpreted as reflecting postformation alteration of the chondrules by either shock disturbance or aqueous alteration (Swindle et al., 1996; Swindle, 1998). Results have been published for chondrules from the ordinary chondrites Semarkona LL3.0 (Swindle et al., 1991a), Chainpur LL3.4 (Swindle et al. 1991b), Parnallee LL3.6 (Gilmour et al., 1995, 2000), Tieschitz H/L3.6 (Nichols et al., 1991), Bjurböle L/LL4 (Caffee et al., 1982b; Gilmour et al., 1995, 2000), and the carbonaceous chondrites Allende CV3 (Swindle et al., 1983; Nichols et al., 1990) and Efremovka CV3 (Swindle et al., 1998). These data (with the exception of that of Tieschitz and Efremovka) are summarized graphically in Figure 4, which, for comparison, also includes the I-Xe ages of two clasts from the Barwell chondrite, which are believed to be igneous in origin (Hutchison et al., 1988; Gilmour et al., 2000), and the ages of feldspars from ordinary chondrites and Acapulco (Brazzle et al., 1999), which are the result of metamorphism. The data illustrated in Figure 4 are referenced to Bjurböle rather than Shallowater because that was the standard adopted in the majority of cases. Experimental uncertainty in calibration of the ^{128}Xe production rate from ^{127}I may have introduced small systematic errors in initial iodine values between different irradiations, and these additional errors have not been included in the figure. I-Xe closure in Shallowater is taken to have occurred 0.66 Ma earlier than in Bjurböle (see section 2.3).

Much of the total range in chondrule ages is accounted for by the Chainpur data, where the authors interpreted the apparent I-Xe correlations as due to shock disturbance after chondrule formation. Disturbance of the I-Xe system in these chondrules is supported by the very low (subsolar) inferred trapped ^{129}Xe/^{132}Xe values reported for several of the Chainpur chondrules. Seventeen chondrules from Semarkona were studied, of which

the majority gave I-Xe ages within (2σ) error of Bjurböle whole rock. Three chondrules from Semarkona formed a cluster of I-Xe ages ~5 Ma later than Bjurböle, suggested by the authors to be a result of aqueous alteration, and a few clustered around a value ~4 Ma earlier. Four chondrules from Parnallee have been studied, of which one (P6) gave a precise age 7.7 Ma later than Bjurböle, one (P32) gave an age comparable to Bjurböle, and two showed poor iodine correlations that could be interpreted as I-Xe ages within error of the Bjurböle standard. I-Xe ages have also been reported for cristobalite-rich objects from Parnallee (Bridges et al., 1993; Gilmour et al., 2000), but these may not be chondrules. Chondrules from Bjurböle generally yield good-quality isochrons that span a range of some 7 Ma centered on the whole-rock value; these have been interpreted as chondrule formation ages.

Only one of the Allende chondrules studied by Swindle et al. (1983) gave an isochron, and it was within 0.5 Ma of the Bjurböle whole-rock standard used. The Allende chondrules studied by Nichols et al. (1990) gave ages from 0.37 Ma earlier than Bjurböle whole rock to 1.4 Ma later.

Although these literature values for I-Xe ages from chondrules have a range in excess of 10 Ma, the later ages can often be shown to be shock artefacts or due to aqueous alteration. The majority of the published ages can be consistently explained as dating closure to diffusion of xenon during cooling immediately subsequent to chondrule formation. This conclusion is supported by the results from this work, in which all chondrule ages were within 2 Ma of the Shallowater standard and date chondrule formation, not subsequent alteration.

There appears to be a real and well-substantiated range in the I-Xe formation ages of chondrules from both the EH3 meteorites studied here and the previously reported data, so whatever the conditions necessary for chondrule formation were, they occurred repeatedly (or continuously) over a period of several million years and in regions of the solar nebula sampled by the parent bodies of enstatite chondrites, ordinary chondrites, and carbonaceous chondrites. Furthermore, the I-Xe formation ages of chondrules bracket the I-Xe age of the Shallowater aubrite (interpreted as due to resetting in an impact between planetesimals; Keil et al., 1989; McCoy et al., 1995) and postdate igneous clasts in Barwell (Hutchison et al., 1988; Gilmour et al., 2000), indicating that differentiated bodies were active at the same time as chondrule formation.

4.3. Chondrule Formation Scenarios

If chondrules did indeed form over a period of a few million years and this interval brackets the formation of ~100-km size and differentiated bodies, what constraints, if any, does this place on the chondrule formation process and environment? Current models of the formation of planetesimal and planet-sized objects (Weidenschilling, 2000) have 1-km objects forming within $\sim 10^4$ yr at 3 AU from an initial dusty environment, and objects of mass 10^{26} g (~3000 km diameter) forming within $\sim 10^6$ yr from such a planetesimal swarm. At this point, half the mass of the original dust remains suspended as fluffy aggregates in gas in the nebula, keeping it optically opaque. It then takes a further 10^8 yr to form objects the size of the terrestrial planets; this final accretionary stage may be accelerated by the loss of nebular gas that would reduce the damping that tended to keep eccentricities low. There is certainly scope within this picture for chondrules to form from "dustball" precursors over a period of a few million years, even if a comparably sized interval is allowed between CAI formation and chondrule formation.

Proposed chondrule-forming events such as accretion shocks, lightning in the nebula, and nebular shocks require a (actively accreting) dusty nebula that is predicted to be the case for ~10 million years (Weidenschilling, 2000; Briceno et al., 2001), although there must be a source for shock generation within the nebula for the latter case. An active pre–main sequence star could provide a source of nebular shocks (by, e.g., FU Orionis outbursts) and later T-Tauri activity could provide energetic solar flares capable of melting solids in the nebula and could be the source of an X-wind capable of exposing material to sufficient solar radiation to cause melting (Shu et al., 1996). Astronomical observations suggest T-Tauri activity of this kind could continue for up to several million years (Feigelson, 1999). The formation of chondrules from an impact melt requires high relative velocities (Taylor et al., 1983), and although it has been suggested that these relative velocities are unlikely to be obtained when there is still significant gas in the nebula, they can occur naturally in the model outlined above after the formation of a planetesimal population due to gravitational stirring. This leads again to a timescale of a few million years for plausible conditions. Other proposed chondrule-forming mechanisms also plausibly occurred over a period of several million years after the formation of the first solids.

It would seem that chondrule formation spanning a few million years is a natural consequence of all the popular models (we are equating the nebular lifetime with a few million years), which are all similarly imprecise about the duration of such events. If chondrules are assumed to be nebular in origin, then the observation that most chondrule formation ages are within 5 million years of each other does suggest that the protosolar nebula did not have a lifetime greatly in excess of this, and this is consistent with astronomical observations (Briceno et al., 2001; Hartmann, 1996). A difficulty with the above is that the range of observed chondrule formation ages is large compared to their dynamical lifetime for drifting into the sun—of the order of 10^5 yr for millimeter-sized objects a few astronomical units from the sun (Cameron, 1995). We must suppose that a fraction of chondrules formed are then somehow stored before final accretion and compaction for $\sim 10^6$ yr on planetesimals large enough to have a significantly greater dynamical lifetime (i.e., $\gg$1 km).

As more chondrule ages of high precision are measured, we will obtain a better idea of the frequency distribution of chondrule formation events, and this, in conjunction with more quantitative modeling, may allow improved discrimination between formation scenarios. An alternative approach to this problem would be to find an independent method of determining the duration of the solar nebula that does not rely on modeling with poorly known boundary conditions and coefficients or on arguments based on chondrule formation ages.

4.4. Implications for the Enstatite Parent Body or Bodies

The difference in ages between the EH and EL subgroups (Kennedy et al., 1988; Wadwha et al., 1997) has been invoked

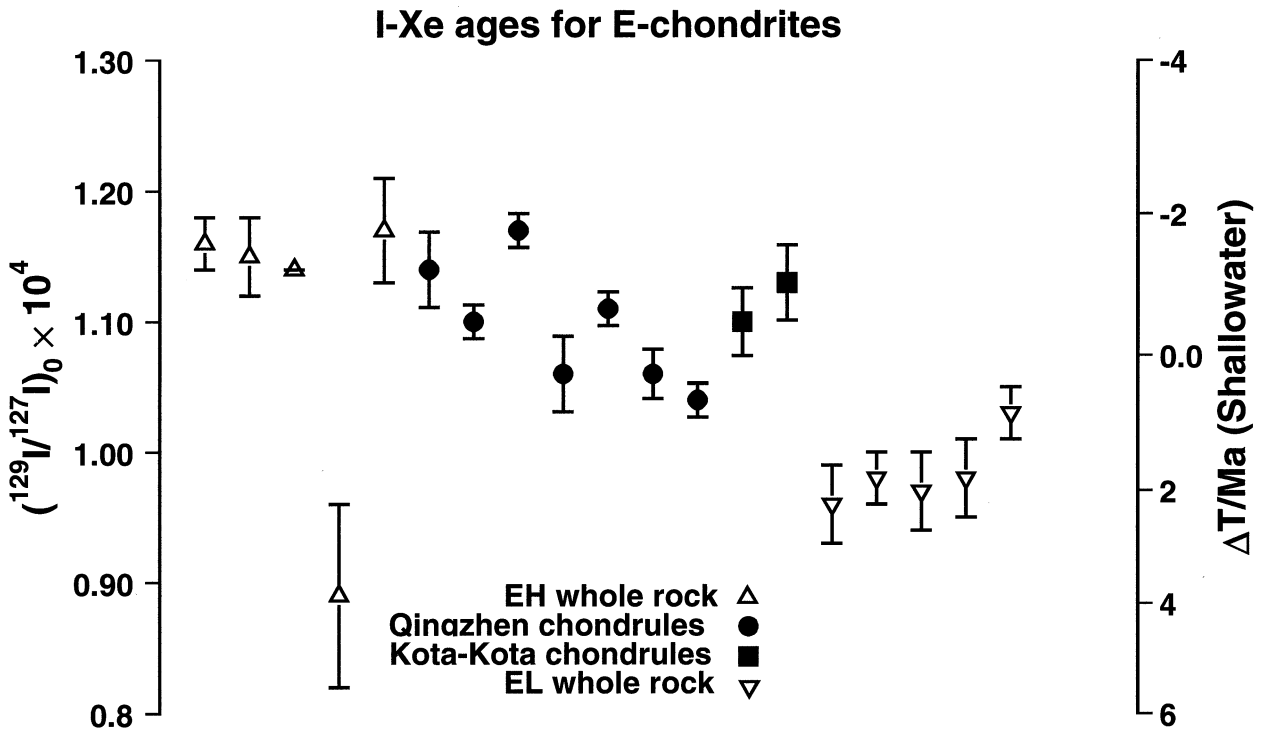

Fig. 5. EH3 chondrule I-Xe ages from this work (solid symbols) and whole-rock enstatite chondrite ages (open symbols) as summarized by Kennedy et al. (1988). The sequence of whole-rock ages is as follows: Indarch EH4, Abee EH4, Kota Kota EH3 (model age), St. Marks EH5, Saint Sauveur EH5, Daniel's Kuil EL6, Hvittis EL6, Blithfield EL6, Khairpur EL6, and Atlanta EL6.

by models both for their formation on a common parent body (Kong et al., 1997) and on separate parent bodies (Keil, 1989). In either case, the observation of components within unequilibrated types having ages that span the previously reported difference between the EH and EL subgroups poses new constraints for these models, although these are readily dealt with in multiple parent-body scenarios. Kong et al. (1997) proposed a single parent-body model consisting of a planetesimal with a layered structure of (proceeding radially inward) EL6, EL3, EH3, EH4, and EH5 arising from heterogeneous accretion together with both internal and external heat sources. This model requires EL material to accrete later than EH material, and so the existence of chondrules within EH3 meteorites that formed as late as some EL whole-rock ages is a problem. However, in this model, low petrologic-type enstatite chondrites are expected to have accreted in a time interval intermediate between higher petrologic-type EH and EL chondrites.

The range of I-Xe ages observed for chondrules from Qingzhen (EH3) and Kota Kota (EH3) in this work span the apparent hiatus in whole rock I-Xe ages between EH and EL chondrites observed by Kennedy et al. (1988). The observation that the EL group closed to xenon diffusion some 4 Ma later than the EH group is supported by results from a Mn-Cr study of sulfides in unequilibrated enstatite chondrites that suggests an age difference of at least 3 Ma between the EH and EL groups (Wadwha et al., 1997). Figure 5 shows the initial iodine values for the chondrules reported in this work, and the whole-rock values observed by Kennedy et al. (1988) for EH and EL chondrites. The only EH3 chondrite included in Kennedy's study was Kota Kota (classified as EH4 at the time), which did not yield a good whole-rock initial iodine value, and so it is not clear whether subcomponents of enstatite chondrites generally span a greater range of initial iodine values than the whole-rock isochrons for a given petrologic type, or whether it is a feature of unequilibrated enstatite chondrites only. Because the sample masses in the I-Xe work reported here were around three orders of magnitude less than in the study by Kennedy et al. (1988), it is likely that a considerable degree of averaging went on to give the apparent whole-rock isochrons.

There is some evidence for scatter in the Mn-Cr ages of individual sulfide grains within single enstatite chondrites (Wadwha et al., 1997). Variations in inferred initial $^{53}Mn/^{55}Mn$ were ascribed to diffusional redistribution of chromium rather than to different formation times on the grounds that an 11-Ma interval between sphalerites within one meteorite was inconsistent with the timescale for accretion of chondritic components. However, we feel that at least some of the variation in initial $^{53}Mn/^{55}Mn$ in sulfides may plausibly be due to formation (or resetting) at different times before assembly and lithification, and that this is consistent with the range of ages for individual chondrules from EH3 meteorites reported in this work.

5. SUMMARY

Chondrules from EH3 meteorites have an observed 2.6-Ma range of I-Xe closure ages, which bracket the I-Xe closure age for enstatite from the Shallowater enstatite achondrite and are

similar to the majority of chondrule ages from ordinary and carbonaceous chondrites. The EH3 chondrule I-Xe ages reported in this work most likely record the cooling of the chondrules shortly after their formation and are not the result of any subsequent processing. If, as proposed by Keil et al. (1989) and McCoy et al. (1995), the I-Xe age of Shallowater enstatite is a result of disruption and reassembly of a 100-km body, then objects of this diameter must have existed at the same time as chondrule formation. The temporal coexistence of bodies of this size with an environment suitable for chondrule formation is predicted by current accretion models and popular chondrule formation theories (cf. section 4.3). This coexistence is required to explain the survival of chondrules formed a few million years apart because of the short dynamic lifetime of such small objects. The recognition that I-Xe chondrule formation ages are similar to I-Xe ages observed for igneous clasts and the impact processing of planetesimals provides a means of coupling the timescales of models for planetesimal accretion and differentiation with those for flash-heating events occurring in the nebula.

Acknowledgments—We thank D. J. Blagburn and B. Clementson for their technical support and R. Burgess for argon analyses of the hornblende monitors. This work was supported by PPARC, by the Royal Society through a University Research Fellowship (J.D.G.), and by the American Museum of Natural History through a Kalbfleisch Research Fellowship (R.D.A.). Considerable improvements were made to the manuscript after receiving thoughtful reviews by Robert Nichols, Tim McCoy. and Charles Hohenberg, and additional comments from Rainer Wieler.

Associate editor: R. Wieler.

REFERENCES

Anders E. and Grevesse N. (1989) Abundances of the elements: Meteoritic and solar. *Geochim. Cosmochim. Acta* **53,** 197–214.

Ash R. D., Gilmour J. D., Whitby J., Prinz M., and Turner G. (1997) I-Xe dating of chondrules from the Qingzhen unequilibrated enstatite chondrite. *Lunar Planet. Sci.* **28, 61–62**.

Brazzle R. H., Kehm K., Hohenberg C. M., Göpel C., Swindle T. D., Davis A. M., and MacPherson G. (1995) I-Xe chronometry: Crock or clock? A program to test and interpret the I-Xe system. *Lunar Planet. Sci.* **26,** 165–166.

Brazzle R. H., Pravdivtseva O. V., Meshik A. P., and Hohenberg C. M. (1999) Verification and interpretation of the I-Xe chronometer. *Geochim. Cosmochim. Acta* **63,** 739–760.

Briceno C., Vivas A. K., Calvet N., Hartmann L., Pacheco R., Herrera D., Romero L., Berlind P., Sanchez G., Snyder J. A., and Andrews P. (2001) The CIDA-QUEST large-scale survey of Orion OB1. Evidence for rapid disk dissipation in a dispersed stellar population. *Science* **291,** 93–96.

Bridges J. C., Franchi I. A., Hutchison R., and Pillinger C. T. (1993) A new oxygen reservoir? Cristobalite bearing clasts in Parnallee [abstract]. *Meteoritics* **28,** 329–330.

Caffee M. W., Hohenberg C. M., Hörz F., Hudson B., Kennedy B. M., Podosek F. A., and Swindle T.D. (1982a) Shock disturbance of the I-Xe system. *J. Geophys. Res.* **87(Suppl.),** A318–A330.

Caffee M. W., Hohenberg C. M., and Swindle T. D. (1982b) I-Xe ages of individual Bjurböle chondrules. *J. Geophys. Res.* **87(Suppl.),** A303–A317.

Cameron A. G. W. (1995) The first ten million years in the solar nebula. *Meteoritics* **30,** 133–161.

Connolly H. C. Jr. and Love S. G. (1998) The formation of chondrules: Petrologic tests of the shock wave model. *Science* **280,** 62–67.

Crabb J. and Anders E. (1981) Noble gases in E-chondrites. *Geochim. Cosmochim. Acta* **45,** 2443–2464.

Crabb J. and Anders E. (1982) On the siting of noble gases in E-chondrites. *Geochim. Cosmochim. Acta* **46,** 2351–2361.

Dodd R. T. (1981) *Meteorites: A Petrologic–Chemical Synthesis.* Cambridge University Press.

El Goresy A., Woolum D. S., Ehlers K., and Ivanov A. V. (1986) Planetary metamorphic events in unequilibrated EH chondrites. *Lunar Planet. Sci.* **17,** 202–203.

El Goresy A., Yabuki H., Ehlers K., Woolum D., and Pernicka E. (1988) Qingzhen and Yamato-691: A tentative alphabet for the EH chondrites. *Proc. NIPR Symp. Antarct. Meteorites* **1,** 65–101.

Emery J. F., Reynolds S. A., and Wyatt E. I. (1972) Half-lives of radionuclides—IV. *Nucl. Sci. Eng.* **48,** 319–323.

Feigelson E. D. (1999) High-energy processes in young stellar objects' *Ann. Rev. Astron. Astrophys.* **37,** 363–408.

General Electric. (1988) *Chart of the Nuclides.* 14th ed. General Electric.

Gilmour J. D. (2000) The extinct radionuclide timescale of the early solar system. *Space Sci. Rev.* **92,** 123–32.

Gilmour J. D., Lyon I. C., Johnston W. A., and Turner G. (1994) RELAX: An ultrasensitive, resonance ionization mass spectrometer. *Rev. Sci. Instrum.* **65,** 617–625.

Gilmour J. D., Ash R. D., Hutchison R., Bridges J. C., Lyon I. C., and Turner G. (1995) Iodine–xenon studies of Bjurböle and Parnallee using RELAX. *Meteoritics* **30,** 405–411.

Gilmour J. D., Whitby J. A., and Turner G. (1997) Comparison of Bjurböle and Shallowater as standards for iodine–xenon dating [abstract]. *Meteorit. Planet. Sci.* **32(Suppl.),** A48.

Gilmour J. D., Whitby J. A., and Turner G. (1998) Xenon isotopes in irradiated ALH84001: Evidence for shock-induced trapping of ancient Martian atmosphere. *Geochim. Cosmochim. Acta* **62,** 2555–2571.

Gilmour J. D., Whitby J. A., Turner G., Bridges J. C., and Hutchison R. (2000) The iodine–xenon system in clasts and chondrules from ordinary chondrites: Implications for early solar system chronology. *Meteorit. Planet. Sci.* **35,** 445–455.

Gilmour J. D. and Saxton J. (2001) Timescales of formation of the first solids. *Phil. Trans. R. Soc. Lond. A,* **359,** 2037–2048.

Hartmann L. (1996) Astronomical observations of phenomena in protostellar disks. In *Chondrules and the Protoplanetary Disk* (eds. R. H. Hewins et al.), pp. 13–20. Cambridge University Press.

Hewins R. H. (1994) Chondrules. *Ann. Rev. Earth Planet. Sci.* **25,** 61–83.

Hewins R. H., Jones R. H., and Scott E. R. D. (1996) *Chondrules and the Protoplanetary Disk.* Cambridge University Press.

Hohenberg C. M. (1967) I-Xe dating of the Shallowater achondrite. *Earth Planet. Sci. Lett.* **3,** 357–362.

Hohenberg C. M. and Kennedy B. M. (1981) I-Xe dating: Intercomparisons of neutron irradiations and reproducibility of the Bjurböle standard. *Geochim. Cosmochim. Acta* **45,** 251–256.

Hohenberg C. M., Pravdivtseva O., and Meshik A. (2000) Reexamination of anomalous I-Xe ages: Orgueil and Murchison magnetites and Allegan feldspar. *Geochim. Cosmochim. Acta* **64,** 4257–4262.

Holden N. E. (1990) Total half-lives for selected nuclides. *Pure Appl. Chem.* **62,** 942–958.

Horanyi M., Morfill G., Goertz C. K., and Levy E. H. (1995) Chondrule formation in lightning discharges. *Icarus* **114,** 174–185.

Hutchison R. H., Williams C. T., Din V. K., Clayton R. N., Kirschbaum C., Paul R. L., and Lipschutz M. E. (1988) A planetary, H-group pebble in the Barwell, L6, unshocked chondritic meteorite. *Earth Planet. Sci. Lett.* **90,** 105–118.

Jessberger E. K. (1983) Ar-Ar ages of carbonaceous and enstatite chondrites [abstract]. *Meteoritics* **18,** 321.

Johnston T. (1995) Relative abundances of chondrule textural types in E3 chondrites. *Lunar Planet. Sci. Conf.* **26, 689–690**.

Kaczaral P. W., Dennison J. E., Verkouteren R. M., and Lipschutz M. E. (1988) On volatile/mobile trace element trends in E3 chondrites. *Proc. NIPR Symp. Antarct. Meteorites* **1,** 113–121.

Kehm K., Nichols R. H., Hohenberg C. M., McCoy T. J., and Keil K. (1993) I-Xe structure of Ilafegh 009 and Shallowater: Evidence for early formation and rapid cooling of impact-derived enstatite meteorites. *Lunar Planet. Sci. Conf.* **24,** 777–778.

Kehm K., Hohenberg C. M., and Nichols R. H. Jr. (1994) Xenon isotopic measurements in Shallowater: In situ pulsed laser volatil-

ization and the search for the carrier of radiogenic ^{129}Xe. *Lunar Planet. Sci. Conf.* **25,**683–684.
Keil K. (1989) Enstatite meteorites and their parent bodies. *Meteoritics* **24,** 195–208.
Keil K., Ntaflos Th., Taylor G. J., Brearley A. J., Newsom H. E., and Romig A. D. Jr. (1989) The Shallowater aubrite: Evidence for origin tk;2lanetesimal impacts. *Geochim. Cosmochim. Acta* **53,** 3291–3307.
Kennedy B. M., Hudson B., Hohenberg C. M., and Podosek F. A. (1988) ^{129}I/^{127}I variations among enstatite chondrites. *Geochim. Cosmochim. Acta* **52,** 101–111.
Kieffer S. W. (1975) Droplet chondrules. *Science* **189,** 333–340.
Kong P., Mori T., and Ebihara M. (1997) Compositional continuity of enstatite chondrites and implications for heterogenous accretion of the enstatite chondrite parent body. *Geochim. Cosmochim. Acta* **61,** 4895–4914.
Langenauer M. and Krähenbühl U. (1993) Depth-profiles and surface enrichment of the halogens in four Antarctic H5 chondrites and in two non-Antarctic chondrites. *Meteoritics* **28,** 98–104.
Lavielle B. and Marti K. (1992) Trapped xenon in ordinary chondrites. *J. Geophys. Res.* **97,** 20875–20881.
Leitch C. A. and Smith J. V. (1982) Petrography, mineral chemistry and origin of Type I enstatite chondrites. *Geochim. Cosmochim. Acta* **46,** 2083–2097.
McCoy T. J., Keil K., Bogard D. D., Garrison D. H., Casanova I., Lindstrom M. M., Brearley A. J., Kehm K., Nichols R. H., and Hohenberg C. M. (1995) Origin and history of impact-melt rocks of enstatite chondrite parentage. *Geochim. Cosmochim. Acta* **59,** 161–175.
Mason B. (1965) The enstatite chondrites. *Geochim. Cosmochim. Acta* **30,** 23–39.
Müller N. and Jessberger E. K. (1985) Laser ^{40}Ar-^{39}Ar dating of the EH3 Qingzhen chondrite. *Lunar Planet. Sci.* **16,**595–596.
Nichols R. H. Jr., Hohenberg C. M., and Olinger C. T. (1990) Allende chondrules and rims: I-Xe systematics. *Lunar Planet. Sci. Conf.* **21,**879–890.
Nichols R. H. Jr., Hagee B.E., and Hohenberg C. M. (1991) Tieschitz chondrules: I-Xe systematics. *Lunar Planet. Sci. Conf.* **21,** 975–976.
Nichols R. H., Hohenberg C. M., Kehm K., Kim Y., and Marti K. (1994) I-Xe Studies of the Acapulco meteorite—Absolute I-Xe ages of individual phosphate grains and the Bjurbole standard. *Geochim. Cosmochim. Acta* **58,** 2553–2561.
Ozima M. and Podosek F. A. (1983) *Noble Gas Geochemistry*. Cambridge University Press.
Podosek F. A. and Cassen P. (1994) Theoretical, observational, and isotopic estimates of the lifetime of the solar nebula. *Meteoritics* **29,** 6–25.
Prior G. T. (1914) The meteorites of Uwet, Kota Kota and Angela: Redeterminations of nickel and iron in the Baroti and Wittekrantz stones. *Min. Mag.* **17,** 129–134.
Rambaldi E. R., Rajan R. S., Murrell M. T., and Burnett D. S. (1984) Coexisting chalcophile and lithophile uranium in Qingzhen (EH3) chondrite [abstract]. *Meteoritics* **19,** 295.
Reynolds J. H. (1960) Determination of the age of the elements. *Phys. Rev. Lett.* **4,** 8–10.
Roddick J. C. (1983) High precision intercalibration of ^{40}Ar-^{39}Ar standards. *Geochim. Cosmochim. Acta* **47,** 887–898.
Rubin A. E. (1997) Mineralogy of meteorite groups. *Meteorit. Planet. Sci.* **32,** 231–247.
Rubin A. E., Scott E. R. D., and Keil K. (1997) Shock metamorphism of enstatite chondrites. *Geochim. Cosmochim. Acta* **61,** 847–858.
Ruzmaikina T. V. and Ip W. H. (1996) Chondrule formation in the accretional shock. In *Chondrules and the Protoplanetary Disk* (eds. R. H. Hewins et al.), pp. 277–284. Cambridge University Press.
Sanders I. S. (1998) A chondrule-forming scenario involving molten planetesimals. In *Chondrules and the Protoplanetary Disk* (eds. R.H. Hewins et al.), pp. 327–334. Cambridge University Press.
Shu F. H., Shang H and Lee T. (1996) Toward an astrophysical theory of chondrules. *Science* **271,** 1545–1552.
Stöffler D., Keil K. and Scott E. R. D. (1991) Shock metamorphism of ordinary chondrites. *Geochim. Cosmochim. Acta* **55,** 3845–3867.
Swindle T. D. (1998) Implications of iodine–xenon studies for the timing and location of secondary alteration. *Meteorit. Planet. Sci.* **33,** 1147–1155.
Swindle T. D., Caffee M. W., Hohenberg C. M., and Lindstrom M. M. (1983) I-Xe studies of individual Allende chondrules. *Geochim. Cosmochim. Acta* **47,** 2157–2177.
Swindle T. D., Grossman J. N., Olinger C. T., and Garrison D. H. (1991a) Iodine–xenon, chemical, and petrographic studies of Semarkona chondrules: Evidence for the timing of aqueous alteration. *Geochim. Cosmochim. Acta* **55,** 3723–3734.
Swindle T. D., Caffee M. W., Hohenberg C. M., Lindstrom M. M., and Taylor G. J. (1991b) Iodine–xenon studies of petrographically and chemically characterized Chainpur chondrules. *Geochim. Cosmochim. Acta* **55,** 861–880.
Swindle T. D., Davis A. M., Hohenberg C. M., MacPherson G. J., and Nyquist L. E. (1996) Formation times of chondrules and Ca-Al–rich inclusions: Constraints from short-lived radionuclides. In *Chondrules and the Protoplanetary Disk* (eds. R. H. Hewins et al.), pp. 77–86. Cambridge University Press.
Swindle T. D., Cohen B., Li B., Olson E., Krot A. N., Birjukov V. V., and Ulyanov A. A. (1998) Iodine–xenon studies of separated components of the Efremovka (CV3) meteorite [abstract 1005]. *Lunar Planet. Sci. Conf.* **29**.
Symes S. J. K. (1997) Problems with arguments against a planetary formation for chondrules [abstract]. *Meteorit. Planet. Sci.* **32,** A127.
Taylor G. J., Scott E. R. D., and Keil K. (1983) Cosmic setting for chondrule formation. In *Chondrules and their Origins* (ed. E. A. King), pp. 262–278. Lunar and Planetary Institute.
Torigoye N. and Shima M. (1993) Evidence for a late thermal event of unequilibrated enstatite chondrites: A Rb-Sr study of Qingzhen and Yamato 6901 (EH3) and Khairpur (EL6). *Meteoritics* **28,** 515–527.
Turner G. (1971) ^{40}Ar-^{39}Ar ages and cosmic ray exposure ages of Apollo 14 samples. *Earth Planet. Sci. Lett.* **12,** 19–35.
Urey H. C. (1967) Parent bodies of the meteorites. *Icarus* **7,** 350–359.
Wacker J. F. and Marti K. (1983) Noble gas components in clasts and separates of the Abee meteorite. *Earth Planet. Sci. Lett.* **62,** 147–158.
Wadwha M., Zinner E. K., and Crozaz G. (1997) Manganese–chromium systematics in sulfides of unequilibrated enstatite chondrites. *Meteorit. Planet. Sci.* **32,** 281–292.
Wang D. and Xie X. (1982) Preliminary investigation of mineralogy, petrology and chemical composition of Qingzhen enstatite chondrite. *Geochemistry* **1,** 69–81.
Weidenschilling S. J. (2000) Formation of planetesimals and accretion of the terrestrial planets. *Space Sci. Rev.* **92,** 295–309.
Weidenschilling S. J. and Marzari F. (1998) Did Jupiter make chondrules? [abstract]. *Meteorit. Planet. Sci.* **33,** A165–A166.
Whitby J. A., Ash R. D., Gilmour J. D., Prinz M., and Turner G. (1997) Iodine–xenon dating of chondrules and matrix from the Qingzhen and Kota Kota EH3 chondrites [abstract]. *Meteorit. Planet. Sci.* **32(Suppl.),** A140
Whitby J. A., Gilmour J. D., and Turner G. (1998) In situ analysis of the iodine–xenon system in a Saharan EH3 chondrite [abstract]. *Meteorit. Planet. Sci.* **33(Suppl.),** A167–168.
Whipple F. L. (1966) Chondrules: Suggestion concerning their origin. *Science* **153,** 54–56.
Wieler R., Anders E., Baur H., Lewis R. S., and Signer P. (1992) Characterisation of Q-gases and other noble gas components in the Murchison meteorite. *Geochim. Cosmochim. Acta* **56,** 2907–2921.
Wood J. A. (1984) On the formation of meteoritic chondrules by aerodynamic drag heating in the solar nebula. *Earth Planet. Sci. Lett.* **70,** 11–26.
Wood J. A. (1996) Unresolved issues in the formation of chondrules and chondrites. In *Chondrules and the Protoplanetary Disk* (eds. R. H. Hewins et al.), pp. 55–69. Cambridge University Press.
York D. (1969) Least-squares fitting of a straight line with correlated errors. *Earth Planet. Sci. Lett.* **31,** 269–278.
Zaikowski A., Jeffery P. M., and Reynolds J. H. (1979) An iodine–xenon study of laboratory-synthesized enstatite. *Lunar Planet. Sci.* **10,** 1395–1397.
Zhang Y. H., Benoit P. H., and Sears D. W. G. (1995) The classification and complex thermal history of the enstatite chondrites. *J. Geophys. Res.* **100,** E9417–E9438.
Zhang Y. H. and Sears D. W. G. (1996) The thermometry of enstatite chondrites: A brief review and update. *Met. Planet. Sci.* **31,** 647–655.
Zolensky M. E., Krot A. N., and Scott E. R. D. (1997) *Workshop on*

Parent-Body and Nebular Modification of Chondritic Materials. LPI Technical Report 97-02, parts 1 and 2. Lunar and Planetary Institute.
Zook H. A. (1980) A new impact model for the generation of the ordinary chondrites. *Meteoritics* **15,** 390–391.

APPENDIX

Petrographic and Mineralogical Descriptions

QC1: Radial Pyroxene (En 68; Ol ~1; Glass 24; SiO_2 4; Metal 2; Sulfide 1)
The enstatite laths are 200 to 300 μm long by ~30 μm wide. They consist of nearly pure enstatite with, at most, 1.0 wt% FeO. In places, the pyroxene encloses forsteritic olivine (Fo98.8 to Fo99.8). The mesostasis consists of material with a feldspathic composition containing up to 11.6 wt% Na; Al contents are fairly uniform between 15.1 and 19.1 wt% and SiO_2 up to 70 wt%. This material also shows extraordinary chlorine abundances, up to 4.0 wt% Cl. The Na and Cl are both heterogeneously distributed, with many areas with Cl levels below detection (<0.01%). Elemental mapping shows that both chlorine and sodium are preferentially enriched along grain boundaries and in cracks. Probe analyses show no clear correlation between the elements, although there is a tendency for spots high in Cl to also be enriched in Na. Potassium is present in high and somewhat variable concentrations (between 0.17 to 0.40 wt%). Fe, Mg, and Ca are also variable but generally only present in low concentrations and do not correlate obviously with each other or with other elements. Mean mesostasis compositions (wt%) are as follows: FeO 0.409 (0.49); MgO 0.91 (1.51); Na_2O 10.65 (1.46); CaO 0.34 (0.27); Al_2O_3 18.12 (0.9); K_2O 0.266 (0.08); Cl 1.28 (1.8).

QC2: Porphyritic Pyroxene–Olivine (Px 56; Ol 13; Glass 26; SiO_2 0; Metal 2; Sulfide 1)
Pyroxene crystals are typically euhedral, 500 × 200 μm, with some smaller porphyritic crystals. The pyroxene is pure enstatite with the FeO content not exceeding 0.6 wt%. The olivines are somewhat smaller, equant grains up to 100 μm in diameter; these too are Mg rich with compositions ranging to only Fo98.9. The mesostasis has a highly variable composition. For example, the sodium content ranges from 2.1 to 10.5 wt% and the Cl content up to 3.4 wt%. It is also Mg rich, up 18 wt% MgO. Mean mesostasis compositions (wt%) are as follows: FeO 0.141 (0.94); MgO 9.10 (5.46); Na_2O 7.16 (2.62); CaO 0.092 (0.026); Al_2O_3 22.06 (1.50); K_2O 1.98 (0.106); Cl 0.98 (0.453).

QC3: Radial Pyroxene (Px 67; Ol 31; SiO_2 0; Metal 0; Sulfide 2)
Pyroxene crystals 10 × 100 μm with interstitial feldspathic glass. A curious feature is that the center is rich in small troilite grains that become less abundant toward the rim. The enstatite grain size also reduces toward the rim. Mean mesostasis compositions (wt%) are as follows: FeO 1.09 (0.56); MgO 28.79 (7.61); Na_2O 1.09 (0.56); CaO 1.44 (0.92); Al_2O_3 4.17 (2.60); K_2O 0.030 (0.018); Cl 0.128 (0.087).

QC4: Radial Pyroxene Silica (Px 68; Ol 0; Glass 13; SiO_2 15; Metal 0; Sulfide 3)
Pyroxene laths up to 200 × 25 μm with small ~10-μm equant silica grains. The pyroxene compositions are variable and can be relatively iron rich, up to 4.6% FeO. The composition of the mesostasis is variable with some areas showing coenrichments of Na (up to 3.4 wt%) and Cl (up to 0.33 wt%) and a more feldspathic composition with up to 7.2% Ca. However, the glass also contains up to 7 wt% FeO. Mean mesostasis compositions (wt%) are as follows: FeO 3.26 (3.02); MgO 13.33 (10.56); Na_2O 1.98 (1.16); CaO 3.61 (2.12); Al_2O_3 10.49 (5.39); K_2O 0.049 (0.027); Cl 0.18 (0.101).

QC5
The entire chondrule was used for I-Xe analysis.

QC6: Radial Pyroxene (Px 74; SiO_2 13; Feldspathic Mesostasis 8; Sulfide 6)
Fine-grained (5 to 20 μm) enstatite containing up to 2.2 to 3.2 wt% FeO. Mesostasis is mostly silica, with some rarer Ca-poor feldspathic regions containing a uniform 10 to 10.5 wt% Na_2O. Abundant small (~10 μm) troilite grains exist in the mesostasis, but there are ~200-μm regions that are porous and sulfide poor, which appear to have had the troilite removed. Mean mesostasis compositions (wt%) are as follows: FeO 0.51 (0.07); MgO 3.48 (1.34); Na_2O 9.51 (0.154); CaO 0.042 (0.0075); Al_2O_3 15.80 (0.119); K_2O 0.118 (0.015); Cl 0.062 (0.03).

QC7: Porphyritic Olivine Pyroxene (Px 51; Ol 21; Glass 24; SiO_2 0; Metal 0; Sulfide 3)
Equant pyroxene grains up to 150 μm across with a single large pyroxene grain more than 800 μm across. Olivines are up to 100 μm but are generally smaller, typically 20 to 50 μm. Held in a Na-rich mesostasis (Na up to 9 wt%) of variable composition that shows clear evidence of partial devitrification, containing small (1 to 2 μm) crystallites, probably of augite. Chlorine content of the mesostasis is up to 0.5 wt% Cl. All mineral phases contain small blebs and stringers of troilite and rare Fe metal. Mean mesostasis compositions (wt%) are as follows: FeO 0.44 (0.202); MgO 4.94 (1.74); Na_2O 7.14 (0.60); CaO 4.99 (1.15); Al_2O_3 19.69 (1.73); K_2O 0.081 (0.017); Cl 0.18 (0.082).

QC8: Porphyritic Olivine-Pyroxene/Radial Pyroxene (Px 20 [Porph]; Ol 23; Groundmass 50; Sulfide 6)
Euhedral olivine and pyroxene up to 600 μm with oldhamite laths up to 500 × 50 μm. The groundmass consists of radial pyroxene (55%) in a silica and feldspathic glass. Glass compositions are difficult to determine due to fine grain size (but see below for low Mg–high Al analyses). Also some fine interstitial sulfide, largely troilite with minor oldhamite and alabandite (MnS). There are also numerous holes that may be due to plucking or to leaching. Mean mesostasis compositions (wt%) are as follows: FeO 0.277 (0.046); MgO 3.12 (3.46); Na_2O 6.97 ((3.76); CaO 0.66 (0.052); Al_2O_3 19.51 (2.24); K_2O 0.299 (0.012); Cl 0.784 0.39).

KC1: Radial Pyroxene (Px 57; Glass 21; SiO_2 10; Metal 4; Sulfide 8)
Enstatite laths radiate from a single point to edge of chondrule, typically 10 μm wide, with occasional thicker cross-cutting enstatite laths. Interstitial material is largely sodic (up to 8% Na_2O) feldspathic material, with some troilite and metal grains (up to 20 × 30 μm). Thick sulfide/metal rim, up to 600 μm thick, 53% troilite, 17% metal, and 27% enstatite, with trace amounts of other sulfides. Mean mesostasis compositions (wt%) are as follows: FeO 0.944 (0.86); MgO 19.11 (7.56); Na_2O 5.79 (1.70); CaO 1.93 (0.05); Al_2O_3 8.173 (2.86); K_2O 0.146 (0.06); Cl 1.41 (0.96).

KC2: Porphyritic Pyroxene/Radial Pyroxene (Px 69; Ol 2; Glass 21; Metal 3; Sulfide 5)
Individual domains up to 150 μm across but made up of crystallites 10 μm across. Some areas show partially resorbed (relic?) olivine grains. The pyroxene composition is near pure enstatite, not exceeding 1.5% mol Fs. The Ca-rich mesostasis contains abundant troilite, up to 30 μm and rarer oldhamite grains up to ~10 μm. Thick sulfide/metal rim up to 400 μm thick. Mean mesostasis compositions (wt%) are as follows: FeO 0.976 (0.71); MgO 18.48 (12.51); Na_2O 4.82 (3.56); CaO 1.25 (1.80); Al_2O_3 9.28 (5.98); K_2O 0.063 (0.036); Cl 0.084 (0.086).

KC3: Radial Pyroxene (Px 63; Glass 20; SiO_2 11; Metal 2; Sulfide 4)
Pyroxene laths up to 400 × 150 μm in Mg-rich feldspathic and silica mesostasis with abundant small (5 μm) troilite and oldhamite grains scattered throughout. Mesostasis has variable composition, up to 14.7 wt% Na_2O and iron from 0.76 to 8.76 wt%. This sample was not used for I-Xe analysis because the sample was lost during preparation. Mean mesostasis compositions (wt%) are as follows: FeO 2.98 (2.48); MgO 10.07 (9.15); Na_2O 7.19 (3.02); CaO 0.18 (0.297); Al_2O_3 10.07 (9.15); K_2O 0.076 (0.028); Cl 0.050 (0.051).

KC4: Radial Pyroxene Olivine (Px 52; Ol 13; Glass 28; SiO_2 0; Metal 2; Sulfide 6)
Enstatite laths radiating from a single point to opposite rim. Some enclose parallel blades of olivine (Fo>99.3) that are in turn bisected by sulfide stringers. The mesostasis has variable sodium (up to 10.7 wt% Na_2O) and low calcium concentrations. Also contains rare Ca-rich pyroxene. Abundant small troilite grains especially in the mesostasis and with some larger interstitial troilite grains and larger troilite and metal grains (to 40 μm) toward the rim. Mean mesostasis compositions (wt%) are as follows: FeO 0.329 (0.142); MgO 13.49 (9.73); Na_2O 6.90 (2.54); CaO 0.621 (1.853); Al_2O_3 12.66 (5.50); K_2O 0.084 (0.043); Cl 0.108 (0.190).